Non-linear Evolution of a Barotropically Unstable Circumpolar Vortex

By Keiichi Ishioka and Shigeo Yoden
Department of Geophysics, Kyoto University, Kyoto 606-01, Japan

(Manuscript received 31 August 1993, in revised form 16 November 1993)

Journal of the Meteorological Society of Japan
Vol. 72, No. 1
Meteorological Society of Japan

Non-linear Evolution of a Barotropically Unstable Circumpolar Vortex

By Keiichi Ishioka and Shigeo Yoden

Department of Geophysics, Kyoto University, Kyoto 606-01, Japan
(Manuscript received 31 August 1993, in revised form 16 November 1993)

Abstract

Non-linear evolution of a barotropically unstable circumpolar vortex, which is an idealization of the polar night jet in the stratosphere, is investigated by numerical time-integrations of a full non-linear vorticity equation over wide ranges of several external parameters of the jet. Some non-linear features which cannot be expected in the linear stability analysis are obtained in the time-integrations.

Two types of stabilization processes are found in diagnosis of the non-linear evolution with daily maps of the absolute vorticity field: The negative gradient of absolute vorticity on the equator-ward side of the jet disappears owing to the vorticity mixing by the growth of thin vortex filaments in middle latitudes, while the negative gradient on the poleward side of the jet disappears owing to the equator-ward displacement of the polar fluid with low absolute vorticity.

Decrease of dominant wavenumber is observed in the non-linear phase of the evolution for wide parameter ranges. An eastward-propagating wave of zonal wavenumber 2 becomes dominant after the stabilization of the circumpolar vortex that is unstable in middle latitudes, even if the exponential growth rate of this wave is not the largest in the linear stability analysis.

1. Introduction

Tracer transport and mixing processes in the stratosphere are currently important and interesting subjects in dynamic meteorology in connection with the ozone hole problem (*e.g.*, McIntyre, 1989, 1990; Holton, 1989). To investigate the mixing processes in detail, high-resolution barotropic models have been used as the most simplified system since Juckes and McIntyre (1987) studied non-linear evolution of a circumpolar vortex disturbed by forced planetary waves of zonal wavenumber 1. They obtained clear evidence of breaking planetary waves and isolation of fluid inside the vortex from the surroundings. Further experiments on the dynamics of the polar vortex have been done with several kinds of two-dimensional models; in particular, Polvani and Plumb (1992) and Yoden and Ishioka (1993) made a "methodical sweep of parameter space" to investigate the sensitivity of the evolution of isolated vortices to experimental parameters using the method of Contour Dynamics/Contour Surgery (CD/CS) and a traditional spectral transform method, respectively.

All of the studies mentioned above are concerned with barotropically stable vortices. On the other hand, Dritschel and Polvani (1992) derived the conditions for the instability of strips of vorticity on the surface of a sphere and illustrated the fully developed stages of the instability by a direct numerical simulation with the CD/CS method. They investigated the roll-up of vorticity strips and obtained the following conclusions; 1) Bands or filaments of vorticity have a more pronounced tendency to roll-up on a sphere than on a plane. 2) Polar vortices are largely ineffective in preventing roll-up instability, particularly in equatorial regions. Although their results give a good theoretical guide for the behavior of filaments of vorticity, those are a little distant from the real atmosphere because the initial vorticity distribution used by them is too simple (piecewise constant for the CD/CS method).

In this paper, thus, we investigate the vorticity mixing at the non-linear phase of the barotropic instability of an idealized polar night jet, wind profile of which was introduced by Hartmann (1983), with a high-resolution spectral model. The instability of the polar night jet is considered to be a possible cause of eastward-moving planetary waves observed in the stratosphere (Hartmann, 1983). Several extensions of the linear stability analysis have been done to investigate the relationship between the instability and the eastward-moving planetary waves (Manney, Nathan and Stanford, 1988, 1989; Manney, Mechoso, Elson and Farara, 1991). These stud-

ies showed the linear unstable modes have similar properties to the observed eastward-moving waves. However, to our knowledge, there are few studies on the non-linear phase of the instability at which the linear unstable modes grow to have a finite amplitude and non-linear interactions become important, except for the work by Kwon and Mak (1988). They investigated the non-linear phase of the instability in a β-channel as a general problem but had no application to the polar night jet.

Our model and experimental procedure are described in Section 2. Results of linear stability analysis and non-linear evolution are given in Section 3. Discussion is in Section 4 and conclusions in Section 5.

2. The model and initial jet profiles

The system under consideration is non-divergent two-dimensional flow on the earth, which flow is governed by the vorticity equation in the form

$$\frac{Dq}{Dt} \equiv \frac{\partial q}{\partial t} + \frac{1}{a^2\cos\varphi}\left(\frac{\partial\psi}{\partial\lambda}\frac{\partial q}{\partial\varphi} - \frac{\partial\psi}{\partial\varphi}\frac{\partial q}{\partial\lambda}\right) = \nu\left(\nabla^2 + \frac{2}{a^2}\right)q, \quad (1)$$

where $q(\lambda,\varphi,t) \equiv \nabla^2\psi + 2\Omega\sin\varphi$ is the absolute vorticity, $\psi(\lambda,\varphi,t)$ the streamfunction, λ the longitude, φ the latitude, t the time, a the radius of the earth ($= 6.37\times10^6$ m), Ω the angular speed of rotation of the earth ($= 7.29\times10^{-5}$/s) and ∇^2 the horizontal Laplacian:

$$\nabla^2 \equiv \frac{1}{a^2}\left[\frac{1}{\cos^2\varphi}\frac{\partial^2}{\partial\lambda^2} + \frac{1}{\cos\varphi}\frac{\partial}{\partial\varphi}\left\{\cos\varphi\frac{\partial}{\partial\varphi}\right\}\right]. \quad (2)$$

The right hand side of Eq. (1) is an artificial viscosity term introduced to smooth numerical behavior, where the conservation law of angular momentum requires the second term of $2/a^2$. If we take a limit of the viscosity coefficient $\nu\to0$, then Eq. (1) states the material conservation law of the absolute vorticity following fluid motion. Throughout this study, we fix the viscosity coefficient ν at a small constant which gives the dissipation time-scale of 1 day at the largest total wavenumber ($N=170$) in our model. That is, $\nu = \dfrac{a^2/\{N(N+1)-2\}}{1\text{ day}} = 1.62\times10^4\,\mathrm{m^2\,s^{-1}}$. As described below, we consider several jets, the peak wind speed (V) and the width (L) of which are of the order of 10^2 m/s and 5×10^6 m, respectively. Then a typical value of the Reynolds number $Re = VL/\nu$ is of the order of 3×10^4, which means that the viscous effect is not important.

The initial jet profiles considered in this paper are the same two types used by Hartmann (1983):

tanh type jet:

$$\overline{u}_0(\varphi) = U\cos\varphi\cdot\frac{1}{2}\left(1+\tanh\frac{\varphi-\varphi_0}{B}\right), \quad (3)$$

Table 1. The e-folding time τ_i(a) and the period τ_r(b) in days for all unstable modes obtained in the linear stability analysis for the tanh type jet with $U=180$ m/s, $B=8°$, and φ_0 varying from 35° to 55°. m is the zonal wavenumber. The most unstable mode is denoted by boldface in (a).

(a)

	m			
φ_0[°]	2	3	4	5
35	48.6	**1.11**	**1.11**	1.85
40	5.65	**1.20**	1.34	3.14
45	3.61	**1.34**	1.76	18.6
50	3.01	**1.59**	2.90	—
55	2.87	**2.10**	13.1	—

(b)

	m			
φ_0[°]	2	3	4	5
35	39.7	3.96	2.14	1.49
40	23.7	3.86	2.14	1.51
45	17.6	3.76	2.14	1.53
50	14.2	3.67	2.16	—
55	12.0	3.62	2.19	—

sech type jet:

$$\overline{u}_0(\varphi) = U\cos\varphi\cdot\mathrm{sech}\frac{2(\varphi-\varphi_0)}{B} \quad (4)$$

where U is a measure of the intensity of the jet, φ_0 the position of it, and B the width of it. Note that the meanings of φ_0 and B are different for each profile. Values of the parameters used in this study are identical to those in Hartmann (1983) and the profiles are illustrated in Figs. 5 and 6 for the tanh type jet and in Figs. 10 and 11 for the sech type jet. The tanh type jets have negative latitudinal gradient of zonal mean absolute vorticity on the equator-ward flank of the jet axis, while the sech type jets have that on the polar flank of it.

The linear stability of the jets is re-examined under the existence of the viscosity term in Eq. (1) with the same spatial resolution as our non-linear model. The stability of a basic zonal flow of $\overline{u}_0(\varphi)$ to an infinitesimal disturbance $\psi'(\lambda,\varphi,t)$ is investigated with a linearized form of Eq. (1) for the disturbance:

$$\left(\frac{\partial}{\partial t} + \frac{\overline{u}_0}{a\cos\varphi}\frac{\partial}{\partial\lambda}\right)\nabla^2\psi' + \frac{1}{a^2\cos\varphi}\frac{d\overline{q}_0}{d\varphi}\frac{\partial\psi'}{\partial\lambda} = \nu\left(\nabla^2+\frac{2}{a^2}\right)\nabla^2\psi', \quad (5)$$

where $\overline{q}_0 \equiv -\frac{1}{a\cos\varphi}\frac{d}{d\varphi}(\cos\varphi\overline{u}_0) + 2\Omega\sin\varphi$. If we assume the disturbance ψ' to take the form;

$$\psi'(\lambda,\varphi,t) = \mathrm{Re}\left\{\sum_{n=m}^{N}\Psi_n^m P_n^m(\sin\varphi)e^{i(m\lambda-\sigma t)}\right\}, \quad (6)$$

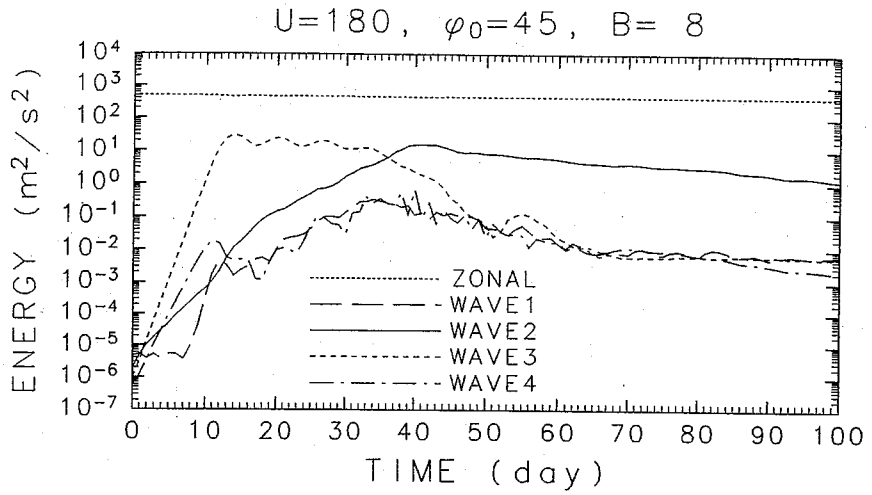

Fig. 1. Evolution of the domain-averaged kinetic energy associated with the zonal flow and Waves 1, 2, 3, and 4 for the standard case of the tanh type jet: $U = 180$ m/s, $\varphi_0 = 45°$, and $B = 8°$.

we finally obtain an algebraic eigenvalue equation. Here P_n^m is the associated Legendre functions defined as;

$$P_n^m(\mu) \equiv \sqrt{(2n+1)\frac{(n-m)!}{(n+m)!}}\frac{(-1)^n}{2^n n!}(1-\mu^2)^{\frac{m}{2}} \times \frac{d^{n+m}}{d\mu^{n+m}}(1-\mu^2)^n. \quad (7)$$

The eigenvalues $\{\sigma\}$ and corresponding eigenvectors of the coefficient matrix are obtained by the QR method.

The non-linear Eq. (1) is numerically integrated from an initial state $q = \bar{q}_0(\varphi) + q_d(\lambda, \varphi)$, where $\bar{q}_0$ is the initial basic zonal flow defined above and $q_d(\lambda, \varphi)$ is an initial disturbance defined as;

$$q_d(\lambda, \varphi) \equiv \alpha\left(e^{\beta(\cos\theta - 1)} - \frac{1 - e^{-2\beta}}{2\beta}\right), \quad (8)$$

$$\cos\theta \equiv \sin\varphi \sin\varphi_d + \cos\varphi\cos\varphi_d\cos(\lambda - \lambda_d). \quad (9)$$

Here α and β are measures of the intensity and horizontal extent of the disturbance, respectively. The center of the disturbance is given by (λ_d, φ_d). We have chosen the initial disturbance, which is a Gaussian-like smooth function on a sphere and has nearly white spectra in the wavenumber space for large β, to investigate behaviors of waves raised by the instability of the basic zonal wind itself. As long as the intensity α is small enough and the parameter β is large enough, the results we obtain are insensitive to the initial disturbance. Throughout this study the disturbance parameters are fixed as $\alpha = 0.01\Omega$, $\beta = 100$, and $(\lambda_d, \varphi_d) = (0°, 45°)$.

The advection term is computed using a spectral transform method with a triangular truncation of T170. The Runge-Kutta-Gill method is used for time-integrations with an increment of 0.01 day.

3. Results

a. Tanh type jet

Table 1 shows the e-folding time $\tau_i = 1/\mathrm{Im}(\sigma)$ and the period $\tau_r = 2\pi/\mathrm{Re}(\sigma)$ of all the unstable modes of wavenumber m for the tanh type jet with $U = 180$ m/s, $B = 8°$, and various values of φ_0. Our results agree with those by Hartmann (1983, Table 4) except for some critical cases in which τ_i is large (or, $\sigma_i \sim 0$). The low-latitude jet ($\varphi_0 = 35°$) favors the growth of high wavenumbers ($m = 3, 4, 5$), while the high-latitude jet ($\varphi_0 = 55°$) favors low wavenumbers ($m = 2, 3$). For high wavenumbers ($m = 3, 4, 5$), τ_i increases as φ_0 increases and vice versa for $m = 2$. Note that Wave 3 has the largest linear growth rate for all φ_0. Period of the unstable waves (τ_r) is not very sensitive to φ_0 except for $m = 2$.

Non-linear evolution of the unstable circumpolar vortex is investigated firstly for the standard case of the tanh type jet with $U = 180$ m/s, $\varphi = 45°$, and $B = 8°$. Figure 1 shows the evolution of the domain-averaged kinetic energy of the zonal flow and four largest wave components defined as;

$$\begin{cases} \text{zonal}: & E_0(t) \equiv \dfrac{1}{4}\displaystyle\int_{-\pi/2}^{\pi/2} \frac{1}{a^2}\left|\frac{d\Psi_0}{d\varphi}\right|^2 \cos\varphi d\varphi \\ \text{wave}: & E_m(t) \equiv \dfrac{1}{2}\displaystyle\int_{-\pi/2}^{\pi/2} \\ & \quad \times\left(\frac{m^2}{a^2\cos^2\varphi}|\Psi_m|^2 + \frac{1}{a^2}\left|\frac{d\Psi_m}{d\varphi}\right|^2\right)\cos\varphi d\varphi \\ & \qquad\qquad (m = 1, 2, \cdots) \end{cases}$$

$$\Psi_m(\varphi, t) \equiv \frac{1}{2\pi}\int_0^{2\pi} \psi(\lambda, \varphi, t) e^{-im\lambda} d\lambda \qquad (m = 0, 1, 2, \cdots)$$

After initial adjustment to the unstable modes, each

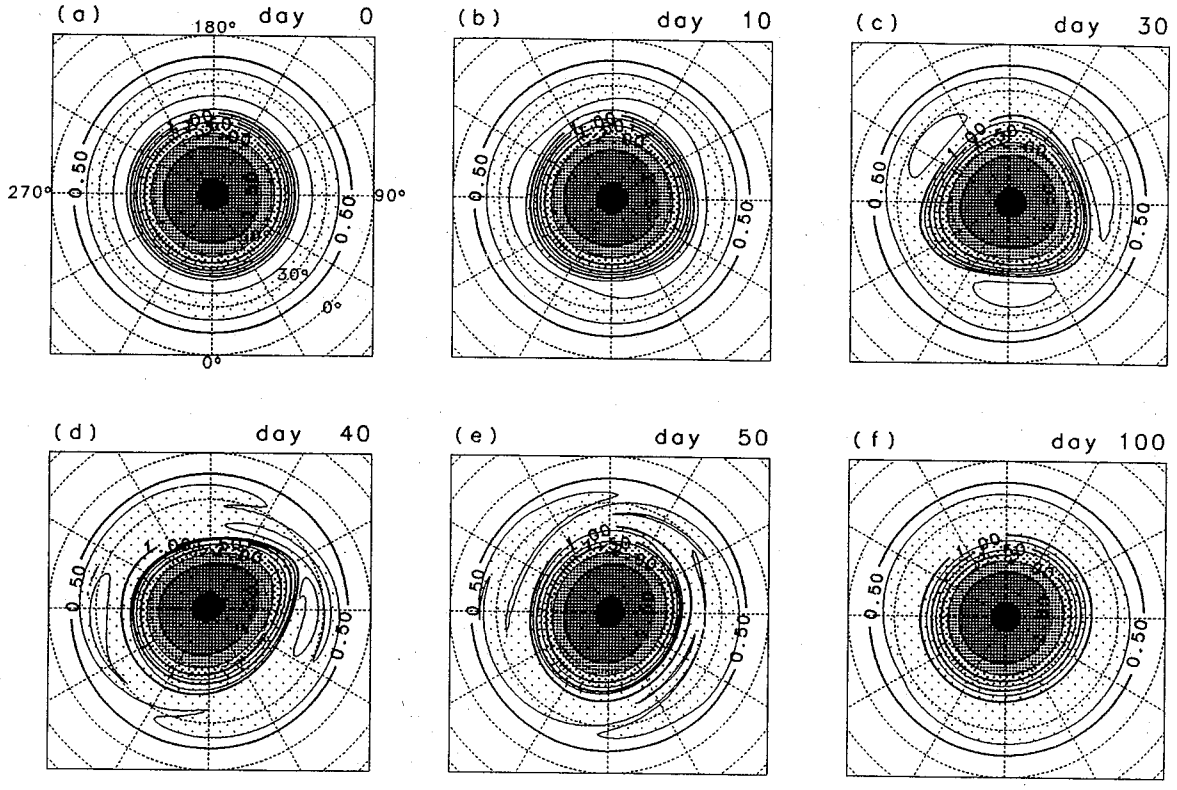

Fig. 2. Evolution of the absolute vorticity (q) field for the standard case of the tanh type jet: $U = 180$ m/s, $\varphi_0 = 45°$, and $B = 8°$. The contour value is scaled by Ω and dark shading corresponds to high q. Lambert equal area projection is used only for a hemisphere ($\varphi \geq 0°$). Meridians and parallels are shown every 30°.

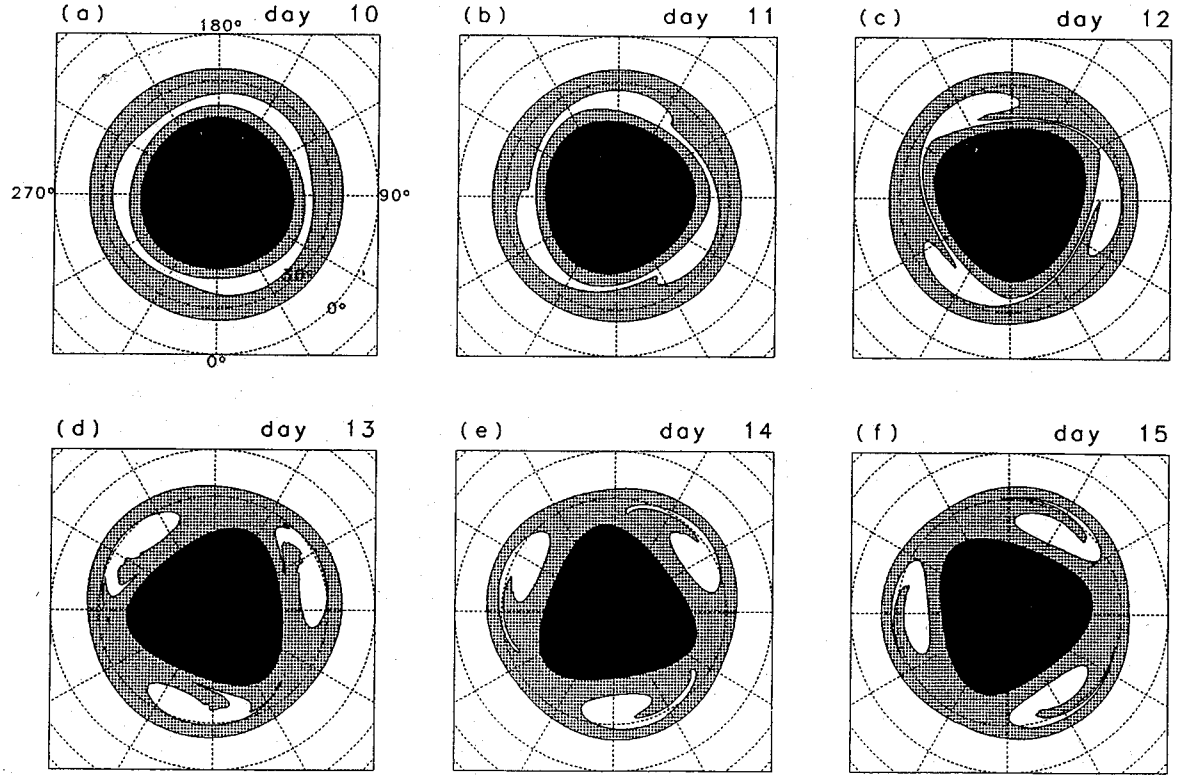

Fig. 3. Day-to-day variation of a limited number of contours of the absolute vorticity (q) field for the standard case of the tanh type jet (Day 10–Day 15). The black area is for $q \geq 1.5\Omega$ and the gray area for $0.75\Omega \leq q \leq 1.5\Omega$.

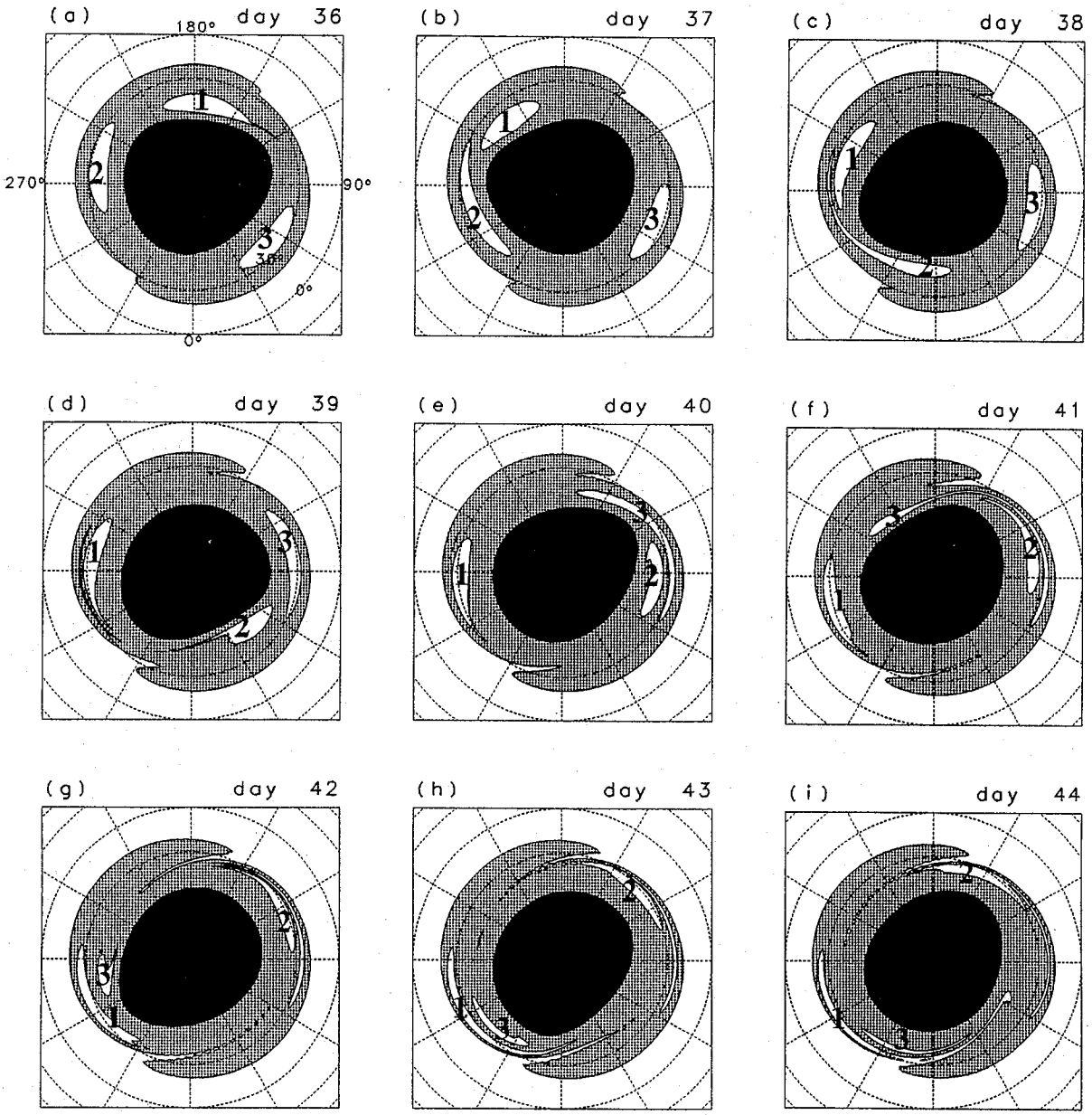

Fig. 4. Same as Fig. 3 except for Day 36–Day 44.

unstable wave, Wave 2, 3, and 4 (Wave 5 is not shown), grows exponentially until Day 10 or so with the rate expected in the linear analysis (Table 1). Afterward, however, non-linearity becomes important. After Day 7, Wave 1 starts growing owing to wave-wave interactions. The exponential growth of Wave 3 halts by Day 14, while Wave 2 keeps growing to exceed Wave 3 at Day 36 and has its maximum at Day 41. The Wave 2 is dominant until the end of the integration, Day 100.

Evolution of the absolute vorticity field $q(\lambda, \varphi, t)$ is shown in Fig. 2. Initially, a zonal band of low q exists around $\varphi = 40°$ (a). The band evolves into three isolated areas of low q until Day 30 corresponding to the growth of Wave 3 (b, c). The growth of Wave 2 distorts the arrangement of the three low q areas at Day 40 (d), and leads to the formation of filament structures in middle latitudes at Day 50 (e). Finally, the fine filaments of absolute vorticity are smoothed out owing to the viscosity and the circumpolar vortex becomes nearly zonally symmetric except for the distortion by Wave 2 (f). At this time the absolute vorticity is an almost monotonically increasing function with latitude in all longitudes.

Day-to-day variations of a limited number of contours are investigated to show the mixing process of absolute vorticity in detail. Figure 3 shows the formation of the three isolated areas of low q from Day

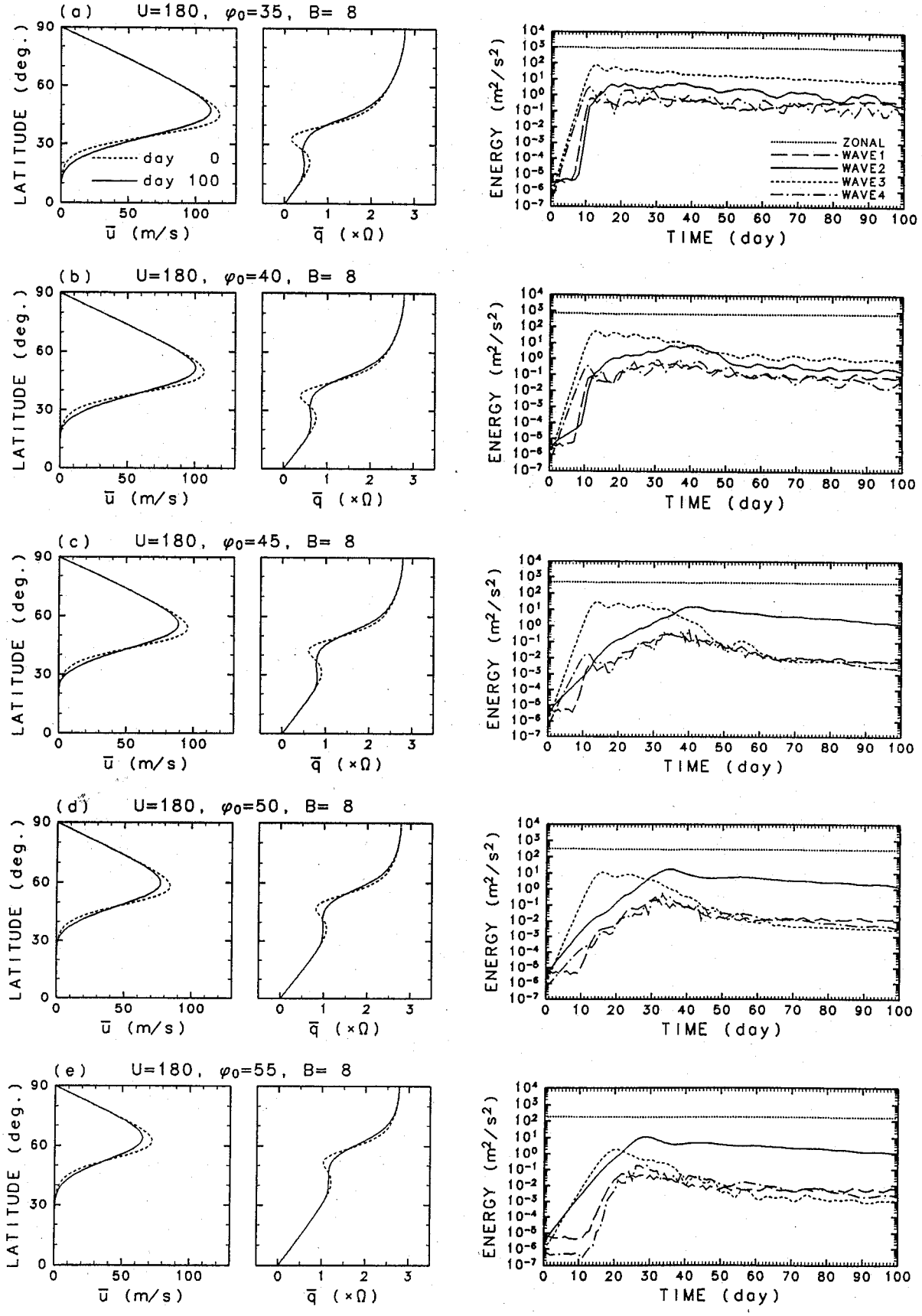

Fig. 5. Sensitivity of the evolution to the latitudinal position parameter φ_0 varying from 35° to 55° for the tanh type jet with $U = 180$ m/s and $B = 8°$. left: $\bar{u}$ profile at Day 0 (dotted line) and Day 100 (solid line), center: $\bar{q}$ profile, right: evolution of the zonal and wave energy.

Table 2. Same as Table 1 except for the sensitivity to the width parameter B of the jet; $U = 180$ m/s and $\varphi_0 = 45°$.

(a)

	m								
B[°]	2	3	4	5	6	7	8	9	10
4	1.17	0.563	0.470	**0.453**	0.479	0.553	0.734	1.14	13.5
6	1.80	0.818	**0.784**	0.980	1.84	—	—	—	—
8	3.61	**1.34**	1.76	18.6	—	—	—	—	—
10	64.9	**3.02**	—	—	—	—	—	—	—
12	—	—	—	—	—	—	—	—	—

(b)

	m								
B[°]	2	3	4	5	6	7	8	9	10
4	12.1	3.29	1.94	1.39	1.09	0.900	0.767	0.675	0.594
6	14.6	3.51	2.03	1.45	1.14	—	—	—	—
8	17.6	3.76	2.14	1.53	—	—	—	—	—
10	21.1	4.05	—	—	—	—	—	—	—
12	—	—	—	—	—	—	—	—	—

10 to Day 15. During the growth of Wave 3, the white band of low q stagnates at three longitudes (a–c). These stagnation regions are separated into three isolated areas owing to the viscosity (d) and roll themselves up into three isolated vortices (e, f).

The process through which Wave 2 dominates over Wave 3 from Day 36 to Day 44 is diagnosed similarly in Fig. 4. At Day 36 (a), the Wave 3 pattern of the main polar vortex (Fig. 3f) is distorted by Wave 2, and the three isolated areas of low q are not spaced equally in longitude. Wave 2 is dominant in low latitudes. One of the isolated areas of low q around $\lambda \sim 180°$ (labeled 1) moves eastward quickly (b). Since the low q area (labeled 1) has clockwise circulation in near fields, another low q area (labeled 2) is stretched around $\lambda \sim 270°$ (c) and the formed filament is cut off (d). The filament is smeared out by the viscosity (e). The remainder of the cut-off low q area (labeled 2) around $\lambda \sim 45°$ in (d) approaches the third one (labeled 3) and stretches it around $\lambda \sim 90°$ (e, f). These catching up processes occur successively to make complicated filament structures (g–i). Note that the thin filaments of low q are piled up at *two* longitudes around $\lambda \sim 150°$ and 330°, corresponding to the predominance of Wave 2 (i).

Similar time-integrations are done for other values of the latitudinal position parameter φ_0. Figure 5 shows the initial and final profiles of zonal mean flow $\overline{u}$ and zonal mean absolute vorticity $\overline{q}$ as well as the evolution of the domain-averaged energy of zonal and wave components for five values of φ_0 listed in Table 1. The middle of the figure (c) is for the standard case already shown above. As the parameter φ_0 increases, maximum value of the initial $\overline{u}$ decreases and latitude of the maximum moves poleward (dotted line in the left column). The corresponding initial $\overline{q}$ is not monotonic with latitude (the center column), satisfying the necessary condition for barotropic instability (Kuo, 1949). The latitudes of negative $d\overline{q}/d\varphi|_{t=0}$ also moves poleward as φ_0 inceases.

These unstable circumpolar jets at the initial state are stabilized by the vorticity mixing in middle latitudes. As a result, $\overline{q}$ is nearly constant in the mixing latitudes and becomes an almost monotonically increasing function at the end of the evolutions. The latitudinal gradient of $\overline{u}$ decreases in middle latitudes corresponding to the change of $\overline{q}$ profiles. Contrarily, $\overline{u}$ and $\overline{q}$ change little out of the mixing latitudes.

The evolutions of each energy (the right column) give information on the dominant wavenumber in linear and non-linear phases. The evolutions are very similar in the cases of high-latitude jet (d, e) and the standard case (c): The energy of Wave 2 exceeds that of Wave 3 in the non-linear phase, although the exponential growth rate of Wave 2 is smaller than that of Wave 3 in the linear phase.

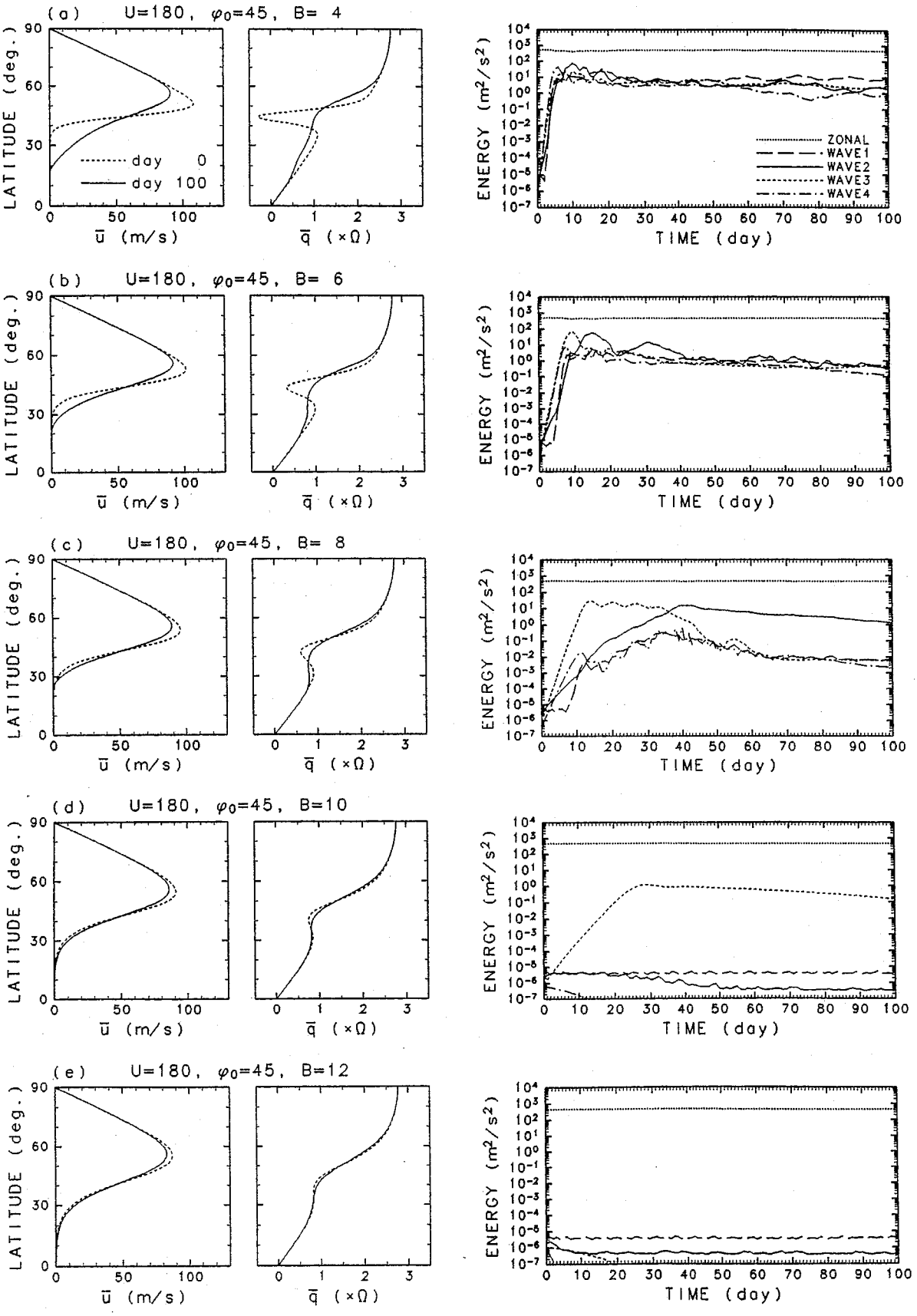

Fig. 6. Same as Fig. 5 except for the sensitivity to the width parameter B varying from 4° to 12° for the tanh type jet with $U = 180$ m/s and $\varphi_0 = 45°$.

Table 3. Same as Table 1 except for the sech type jet with $B = 20°$, $\varphi_0 = 60°$, and U varying from 120 m/s to 240 m/s.

(a)			(b)		
	m			m	
U [m/s]	1	2	U [m/s]	1	2
120	**8.88**	18.2	120	4.72	2.51
150	**7.02**	11.0	150	3.67	1.97
180	**5.90**	7.96	180	3.00	1.62
210	**5.13**	6.26	210	2.53	1.38
240	**4.57**	5.17	240	2.19	1.20

Wave 2 is dominant at the end of the evolution for these cases. An excess of the energy of Wave 2 is observed even in the case of $\varphi_0 = 40°$ (b) for a short period. Only in the lowest latitude case of $\varphi_0 = 35°$ (a), Wave 3 is predominant through the evolution. The q field analysis is also done for these experiments (not shown). For the three evolutions in which the Wave 2 becomes dominant (c–e), the formation of vorticity filaments due to the catching-up processes of three low q areas are observed in the similar way as shown in Figs. 2, 3 and 4. On the other hand, the catching-up processes are not observed clearly in the low-latitude jet cases (a, b), although similar three isolated low q areas are formed as shown above.

Sensitivity of the linear stability and non-linear evolutions to the width parameter B is also investigated for the tanh type jet.

Table 2 summarizes the linear stability analysis for the jet with $U = 180$ m/s, $\varphi_0 = 45°$, and B varying over the values 4°, 6°, 8°, 10°, and 12°. For the narrowest case of $B = 4°$, the circumpolar jet is unstable for many zonal wavenumbers of $m = 2, 3, \cdots, 10$. The number of unstable modes decreases as the width parameter increases. When $B = 12°$, the jet is stable. The wavenumber of the most unstable mode becomes small as the width of the jet increases; Wave 5 is most unstable for $B = 4°$, Wave 4 for $B = 6°$, and Wave 3 for $B = 8°$ and 10°.

Figure 6 shows the dependence of evolutions on the width parameter B. The middle of the figure (c) is the standard case again. The negative gradient of the initial $\overline{q}$ profiles in (a)–(d) disappears owing to the vorticity mixing by the unstable waves as in Fig. 5. However, the change of $\overline{q}$ profile in (e) is solely due to the viscosity, because the jet is stable. For the narrow jet cases of $B = 4°$ and 6° (a, b), the competition of the unstable waves occurs similarly to the standard case (c); the energy of Wave 2 exceeds that of Wave 3 and 4 which have larger growth rates initially. In the narrowest jet case (a), the competition is very complicated because there are many unstable modes (see Appendix for the q field analysis of the narrowest case). For a wide jet case of $B = 10°$ (d), such a competition is not seen; only Wave 3 grows to be equilibrated with the zonal mean flow, and the weakly unstable Wave 2 has no substantial role in the evolution.

b. Sech type jet

The sech type jet whose profile is given by Eq. (4) has negative latitudinal gradient of $\overline{q}$ in the polar region as shown in Figs. 10 and 11. Table 3 shows the properties of all linear unstable modes for the sech type jet with $B = 20°$, $\varphi_0 = 60°$, and the five values of U, 120 m/s, 150 m/s, 180 m/s, 210 m/s, and 240 m/s. For all these values of U, the jet is unstable with respect to only Wave 1 and Wave 2;

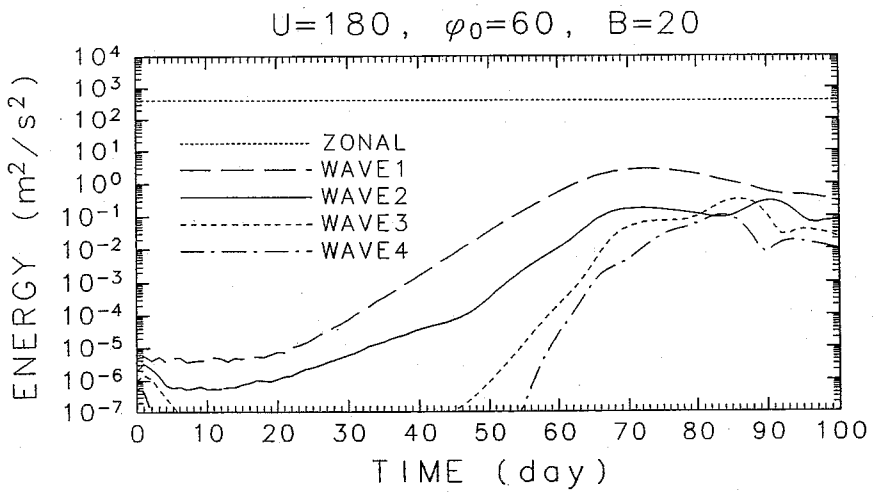

Fig. 7. Same as Fig. 1 except for the standard case of the sech type jet: $U = 180$ m/s, $\varphi_0 = 60°$, and $B = 20°$.

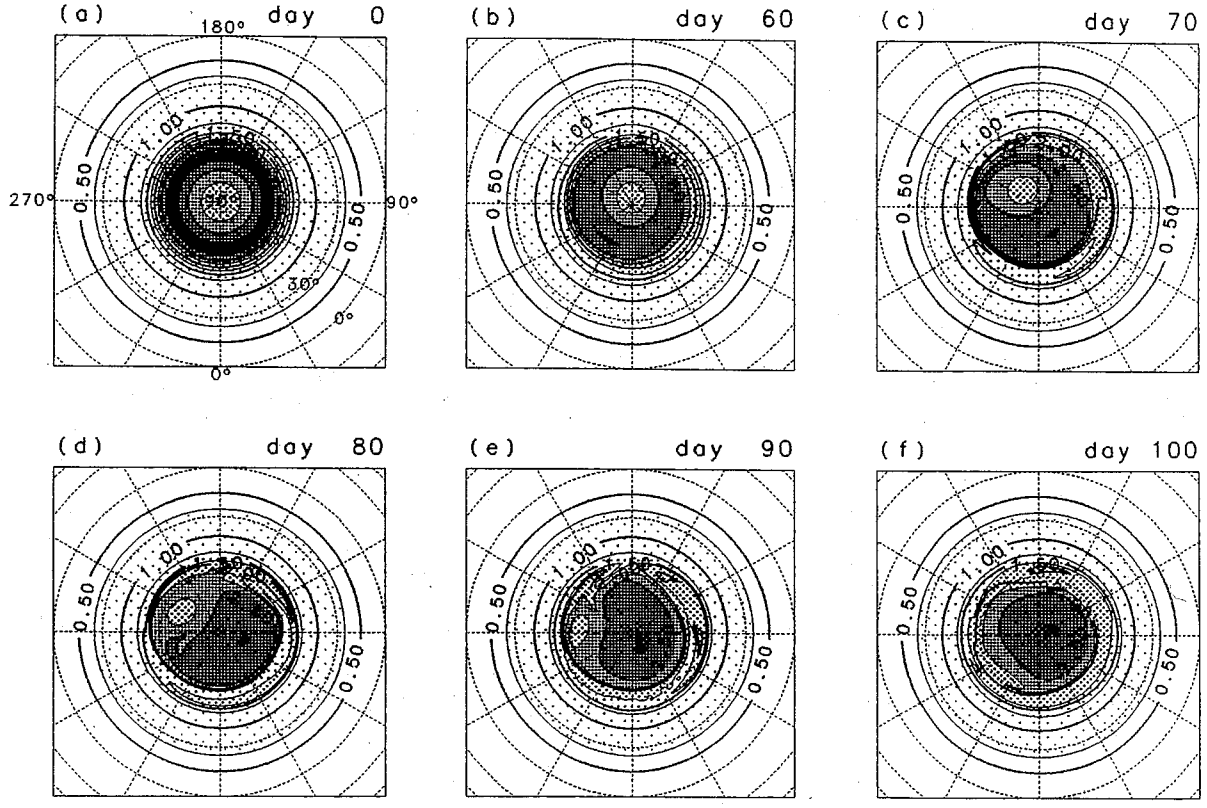

Fig. 8. Same as Fig. 2 except for the standard case of the sech type jet: $U = 180\,\mathrm{m/s}$, $\varphi_0 = 60°$, and $B = 20°$.

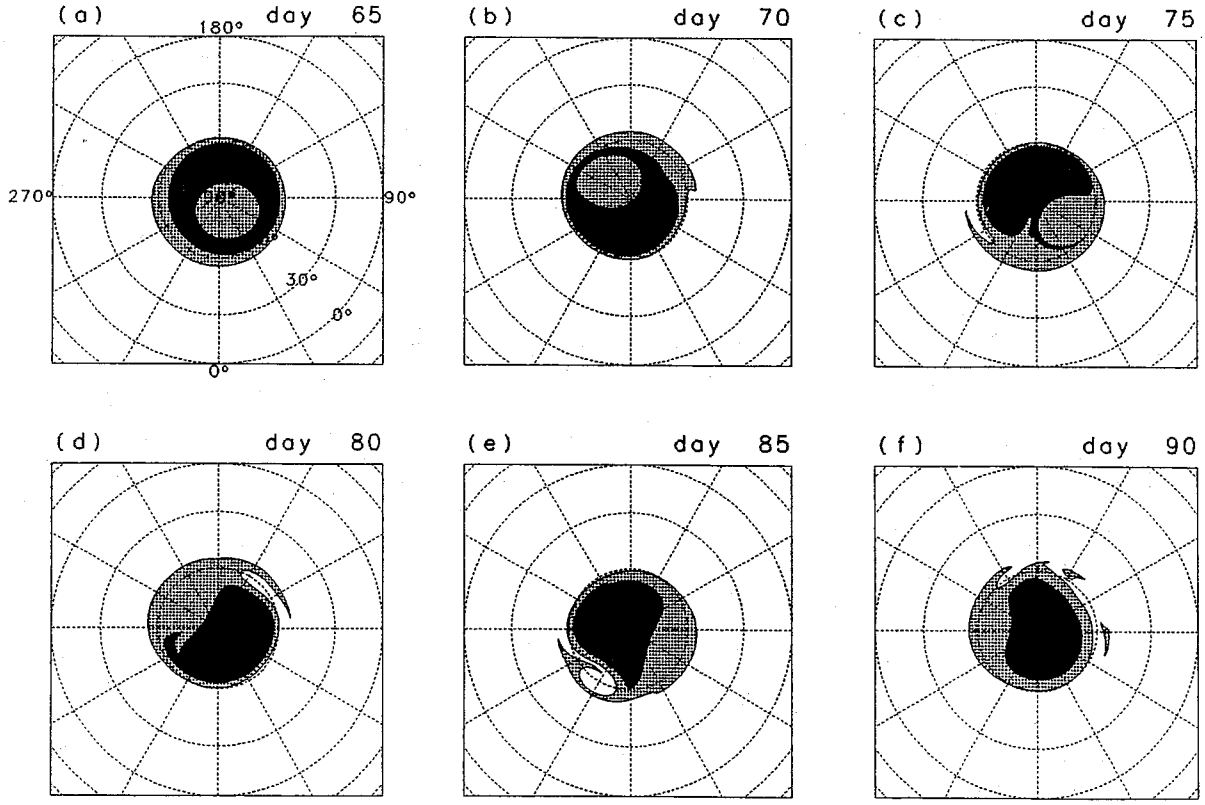

Fig. 9. Time variation of a limited number of contours of the absolute vorticity (q) field for the standard case of the sech type jet (every 5 days from Day 65 to Day 90). The black area is for $q \geq 2.5\Omega$ and the gray area for $2.0\Omega \leq q \leq 2.5\Omega$.

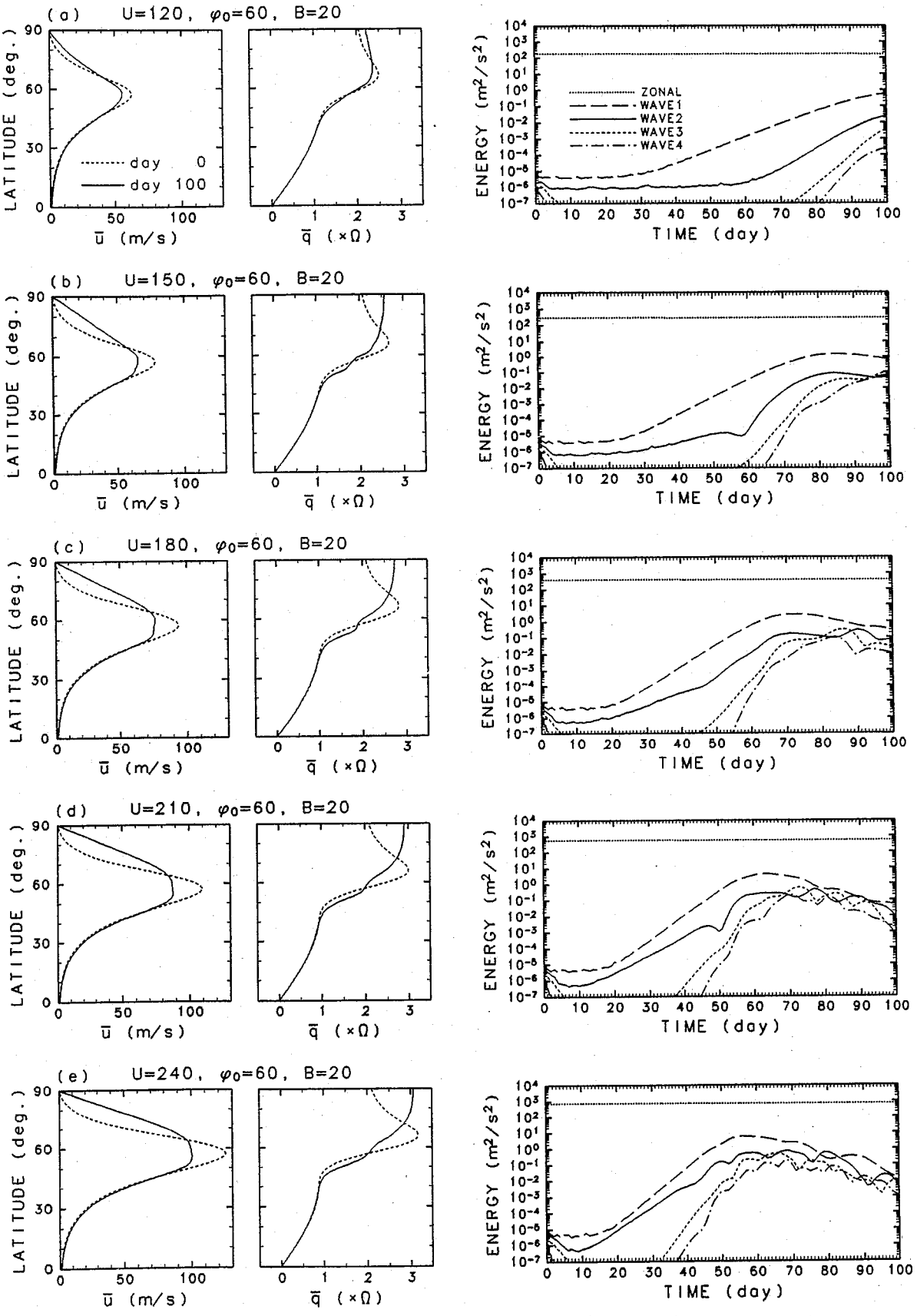

Fig. 10. Same as Fig. 5 except for the sensitivity to the intensity parameter U varying from 120 m/s to 240 m/s for the sech type jet with $\varphi_0 = 60°$ and $B = 20°$.

Table 4. Same as Table 3 except for the sensitivity to the width parameter B of the jet; $U = 180$ m/s and $\varphi_0 = 60°$. Values in parenthesis are for mid-latitude modes.

(a)

	m						
B[°]	1	2	3	4	5	6	7
10	4.82	2.65	3.22	10.1	—	—	—
	(—)	(6.41)	(1.21)	**(1.08)**	(1.38)	(2.82)	(67.4)
15	5.11	**4.22**	21.4	—	—	—	—
	(—)	(—)	(4.97)	(—)	(—)	(—)	(—)
20	**5.90**	7.96	—	—	—	—	—
25	**7.03**	20.9	—	—	—	—	—
30	**8.51**	—	—	—	—	—	—

(b)

	m						
B[°]	1	2	3	4	5	6	7
10	2.93	1.65	1.15	0.877	—	—	—
	(—)	(16.2)	(3.19)	(1.68)	(1.11)	(0.813)	(0.614)
15	2.97	1.65	1.12	—	—	—	—
	(—)	(—)	(2.79)	(—)	(—)	(—)	(—)
20	3.00	1.62	—	—	—	—	—
25	3.01	1.60	—	—	—	—	—
30	3.01	—	—	—	—	—	—

Wave 1 grows more rapidly. Both the e-folding time τ_i and the period τ_r decrease as U increases.

Figure 7 shows the evolution of the domain averaged energy for the standard case of the sech type jet ($U = 180$ m/s, $B = 20°$, and $\varphi_0 = 60°$). Initially, Wave 1 and Wave 2 grow little because the initial disturbance is not the unstable eigenmode. The linear unstable modes become significant and the wave energy grows exponentially after Day 20 or so. Non-linearity becomes important after Day 45 when Wave 2 increases its growth rate and Wave 3 and Wave 4 grow rapidly owing to wave-wave interactions. The growth of Wave 1 halts around Day 70, but other waves do not surpass Wave 1 throughout the evolution.

Evolution of the absolute vorticity field is shown in Fig. 8. Initially, the fluid of low absolute vorticity exists over the pole (a). Corresponding to the growth of Wave 1, the fluid shifts off the pole toward low latitude (b, c). After this displacement, the fluid of lower absolute vorticity merges into the outer region (d, e). Finally, the absolute vorticity is monotonically increasing with latitude at any longitude (f).

Figure 9 emphasizes this displacement of the polar fluid and the merger process from Day 65 to Day 90 by reducing the number of contours. During the period of the displacement (a, b), the low q fluid near the polar region moves eastward with an angular speed of 360°/3 days. Remember that the angular speed ($360°/(m\tau_r)$) of both unstable modes of Wave 1 and Wave 2 is close to this value (Table 3b). Just before Day 75 (c), thin high-q band around $\lambda \sim 80°$ disappears owing to the viscosity, and the polar fluid merges into the outer region of the same absolute vorticity. If there were no viscosity as assumed in the CD/CS method, the polar fluid would be topologically isolated from the outer region. After the merger process some small filaments are formed around 60° latitude (c–e). However, the filamentation and mixing are not very impressive compared with the cases for tanh type jets (Fig. 4).

Figure 10 summarizes the dependence of evolutions on the intensity parameter U; U is varied from 120 m/s (a) to 240 m/s (e) and the middle (c) corresponds to the standard case. The initial $\overline{q}$ profile has a negative gradient in high latitudes for all the

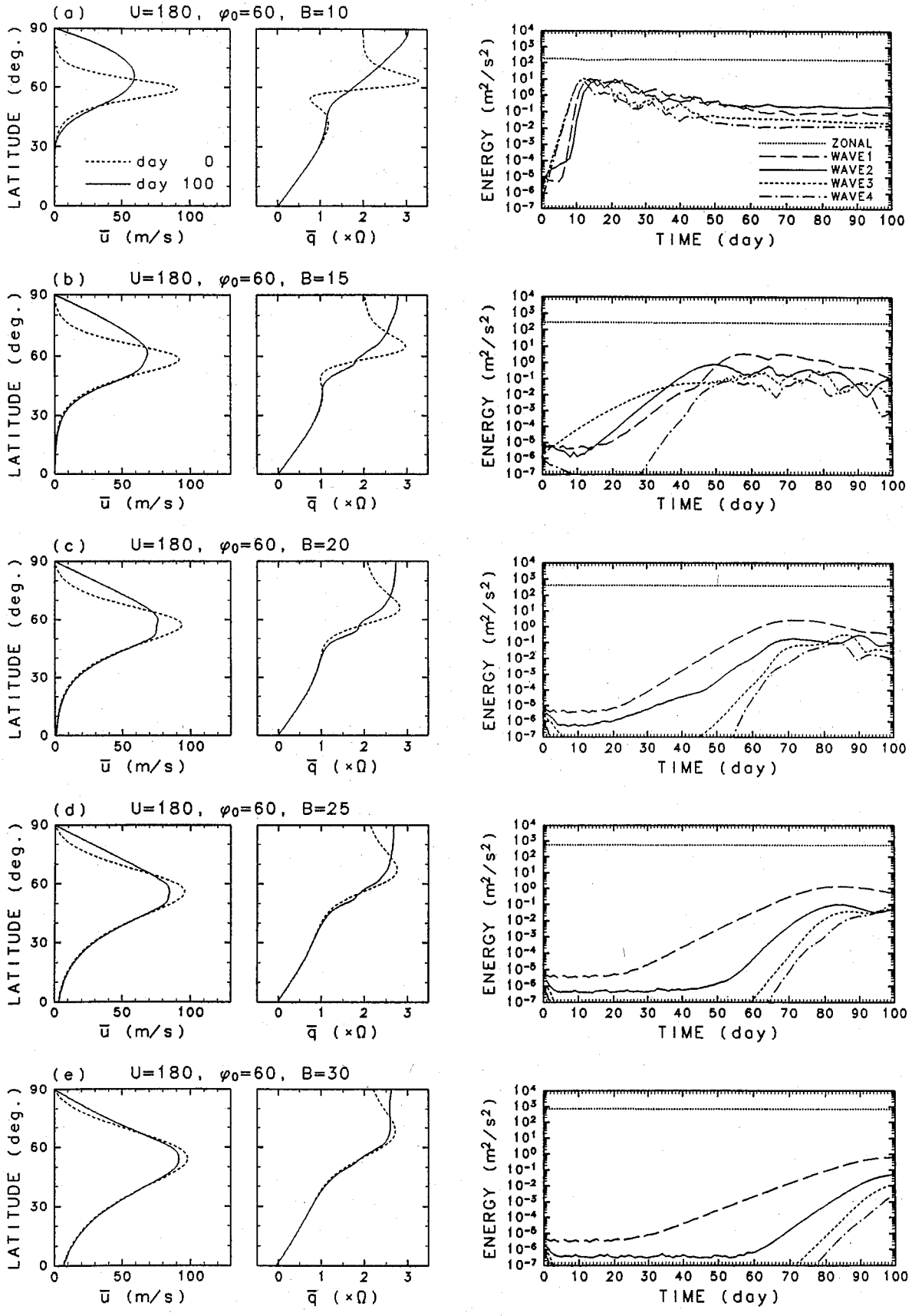

Fig. 11. Same as Fig. 5 except for the sensitivity to the width parameter B varying from 10° to 30° for the sech type jet with $U = 180$ m/s and $\varphi_0 = 60°$.

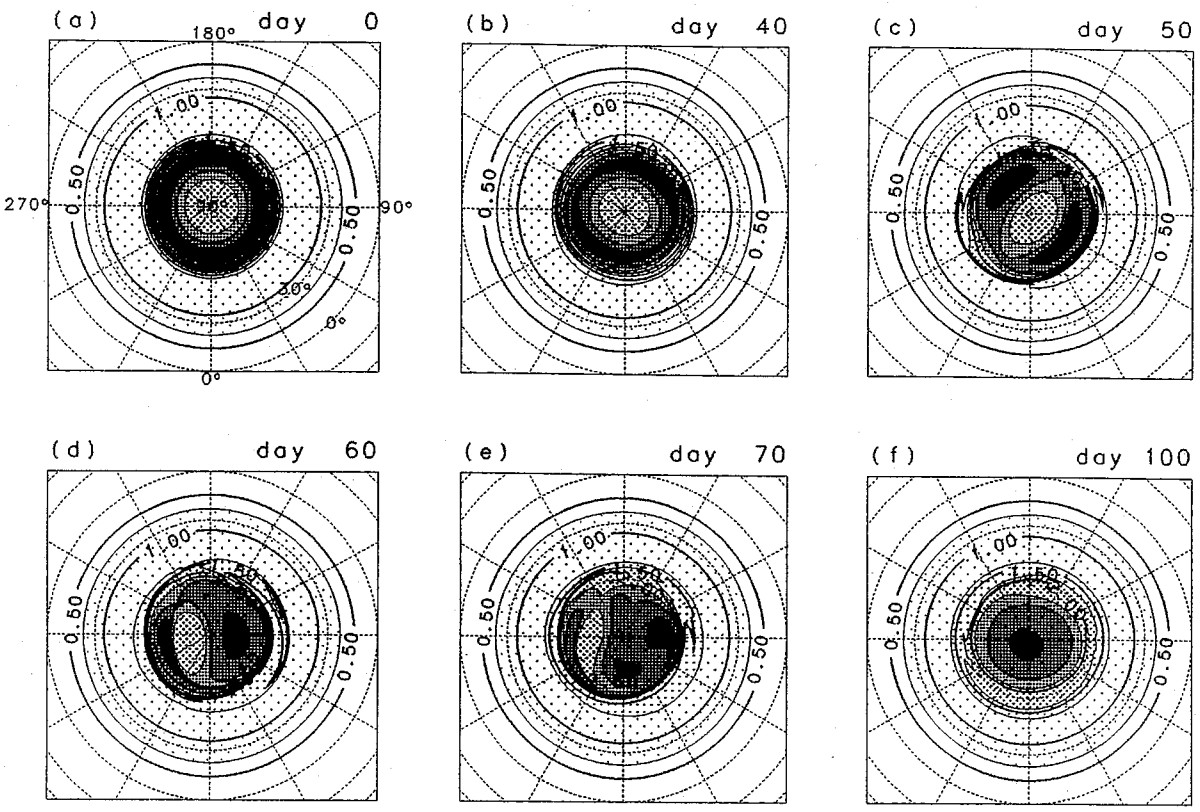

Fig. 12. Same as Fig. 2 except for the sech type jet with $U = 180$ m/s, $\varphi_0 = 60°$, and $B = 15°$.

cases. Similarly to the standard case, these negative gradients of $\overline{q}$ disappear owing to the equator-ward displacement of the low q polar fluid except for the weakest case (a), in which the displacement is not accomplished yet at the end of integration (Day 100). Corresponding to this change of absolute vorticity, the jet becomes weak and wide. For these five cases, the most unstable Wave 1 is dominant in the non-linear phase of evolution. The competition of the unstable waves is not observed in contrast to the tanh type jets.

Sensitivity of the linear stability and non-linear evolutions to the width parameter B is also investigated for the sech type jet given by Eq. (4).

Table 4 summarizes the linear stability analysis for the jet with $U = 180\,\mathrm{m/s}$, $\varphi_0 = 60°$, and B varying over the values 10°, 15°, 20°, 25°, and 30°. Two kinds of unstable modes are obtained for the narrow jets ($B = 10°$ or 15°), because the initial $\overline{q}$ profile has negative gradients in middle latitudes as well as in high latitudes (Fig. 11). The mode that originates from the negative gradient in middle latitudes, which is called "mid-latitude mode", has a longer period as pointed out by Hartmann (1983) (the τ_r values in parenthesis in Table 4 for $B = 10°$ or 15°).

Figure 11 shows the dependence of evolutions on the width parameter B. The middle (c) is the standard case again. The negative gradient of $\overline{q}$ disappears owing to the equator-ward displacement of the low q polar fluid and the jet becomes weak and wide. Non-linear evolution for the cases of wide jet (d, e) is very similar to the standard case, in which the most unstable Wave 1 is dominant as shown in Figs. 8 and 9. On the other hand, the competition between unstable waves is observed for the cases of narrow jets (a, b). The linear stability analysis is not very useful to forecast the non-linear evolution for these cases as in the cases of tanh type jet. In the narrowest jet case (a), the competition is very complicated because there are many unstable modes. See Appendix for the q field analysis of the narrowest case.

Figure 12 shows another example of the competition in the evolution of q field corresponding to Fig. 11b of $B = 15°$. Firstly, the low q area in the polar region is stretched out by the growth of Wave 2 (b, c). The stretched low-q area shifts off the pole owing to the growth of Wave 1 (d) and merges into the outer region (e). Finally, the nearly zonally symmetric circumpolar vortex appears (f). Filamentation and small-scale mixing are not very significant as in the standard case of sech type jet.

4. Discussion

In the non-linear evolutions of barotropically unstable circumpolar vortex over wide ranges of exter-

nal parameters, we observed that the waves which have smaller zonal wavenumbers than the most unstable mode tend to dominate. For example, Wave 2 dominates Wave 3 in Fig. 5c–5e for tanh type jet and Wave 1 exceeds Wave 2 in Fig. 11b for the sech type jet. Such competitions among unstable waves occur when the wave of smaller wavenumber has a little smaller growth rate than the most unstable mode (see Tables 1 and 4 for the above examples). This scale selection in the non-linear evolution of barotropically unstable flow has been already reported by Niino and Misawa (1984) with a laboratory experiment and Kwon and Mak (1988) with a numerical experiment. As Niino and Misawa (1984) discussed, the mechanism of the scale selection can be conjectured as follows: Initially, the most unstable wave grows and stabilizes the unstable basic state to a certain extent. Owing to this stabilization, the wave stops growing to result in a nearly equilibrated state such as Figs. 2c and 12b. However, the nearly equilibrated state is still unstable for waves of smaller wavenumber, and these waves keep growing to stabilize the flow completely. As a result, the wave that has the largest growth rate in the linear stability analysis is often dominated by the waves of smaller wavenumbers.

The transition process of dominant wavenumber has an important role in the mixing of absolute vorticity q in the cases of tanh type jet. As shown in Fig. 3 the growth of Wave 3 makes the low q area in middle latitudes roll up into three isolated vortices. Such rolling up associated with the barotropic instability has been already described by Dritschel and Polvani (1992) with the CD/CS method. However, absolute vorticity is not mixed sufficiently until Wave 2 grows to distort the absolute vorticity field and the interaction between the low q vortices produces the filament structures (Fig. 4). In other words, the reason why the nearly equilibrated state of zonal flow with Wave 3 (Fig. 2c) allows Wave 2 to grow may be that the growth of Wave 2 promotes the vorticity mixing as shown in Fig. 4. Applying such an explanation to the sech type jet, the transition from the Wave 2 pattern in q field into Wave 1 pattern in Fig. 12 is considered to be due to the insufficiency of the vorticity mixing (or rearrangement) by Wave 2 at the stage of Fig. 12b.

It is not straightforward to apply the present results to the real stratosphere, because our model is a conserved system without any forcing or dissipation and our initial state is an idealized zonally symmetric vortex with very small disturbance. However, there are some interesting similarities between our results and observations. Satellite observation shows the fact that the eastward-propagating Wave 2 is usually dominant in middle latitudes in the southern hemisphere stratosphere during winter and spring (Harwood, 1975; Hartmann, 1976). The observational fact is inconsistent with the linear stability analysis of the tanh type jet shown in Tables 1 and 2. Even if some realistic zonal flows of the winter stratosphere in the southern hemisphere are used as the basic flow, the mid-latitude mode of Wave 3 usually has the largest growth rate (Manney *et al.*, 1991). To reconcile this discrepancy, Manney *et al.* (1991) made a linear stability analysis of a realistic baroclinic jet with both latitudinal and vertical shears to show that Wave 2 usually has the largest growth rate when the realistic vertical structure is included. That is, in their linear study, baroclinicity of the basic flow is necessary to explain the dominance of Wave 2 in the real atmosphere. However, our result that Wave 2 often exceeds Wave 3 in nonlinear stage of the barotropic instability as shown in Fig. 5b–5e and Fig. 6b, 6c for the tanh type jet may give another explanation of the dominance of Wave 2 in the southern hemisphere stratosphere. However, further investigations with forced-dissipative systems are necessary to apply the present results to the real stratosphere.

Another similarity between our results and observations is seen in the stabilization process of the sech type jet. As shown in Fig. 9, the lower absolute vorticity fluid in the middle of the polar vortex shifts off the pole and merges into the outer region to stabilize the circumpolar vortex. Such a stabilizing process seems to be a special feature of the instability in a spherical geometry. During the displacement, the "patch" of the lower absolute vorticity keeps its material entity until it merges into the outer region. This nondispersive vortex patch may correspond to the "warm pool" circling the pole with a period of nearly 4 days, which is reported by Prata (1984) and Lait and Stanford (1988).

5. Conclusions

Evolution of a barotropically unstable circumpolar vortex with a jet structure was investigated by a linear stability analysis and time-integrations of a full non-linear vorticity equation in a spherical domain. Two idealized jet profiles introduced by Hartmann (1983) were investigated over wide ranges of some parameter values: a tanh type jet for the mid-latitude modes and a sech type jet for the polar mode. Non-linear stabilization processes of the two types of the polar vortex show some features which cannot be expected by the linear stability analysis.

1. When an unstable circumpolar vortex of the tanh type jet is stabilized by wave disturbances, the negative gradient of zonal mean absolute vorticity on the equator-ward side of the jet disappears owing to the vorticity mixing by the filaments formed through the interactions between some isolated vortices (Fig. 4). For the sech type jet, on the other hand, the negative

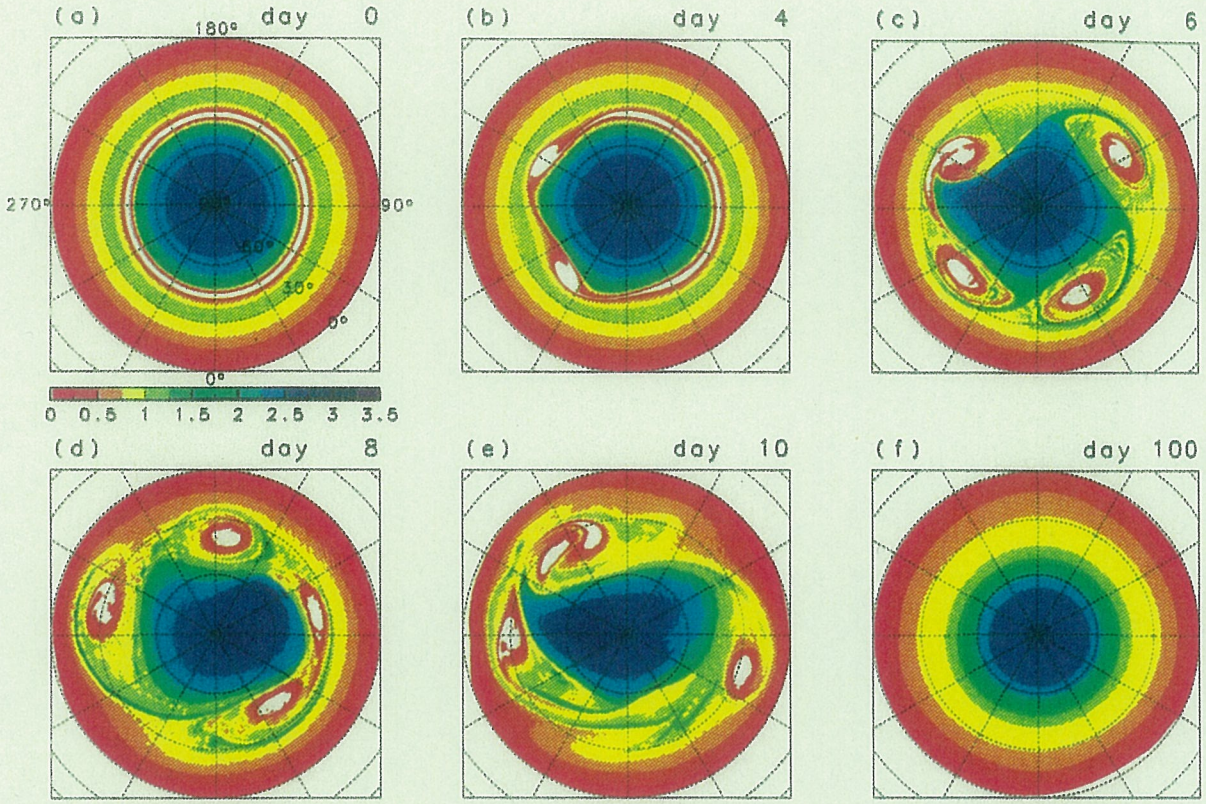

Fig. A1. Evolution of the absolute vorticity field for the tanh type jet with $U = 180\,\mathrm{m/s}$, $\varphi_0 = 45°$, and $B = 4°$.

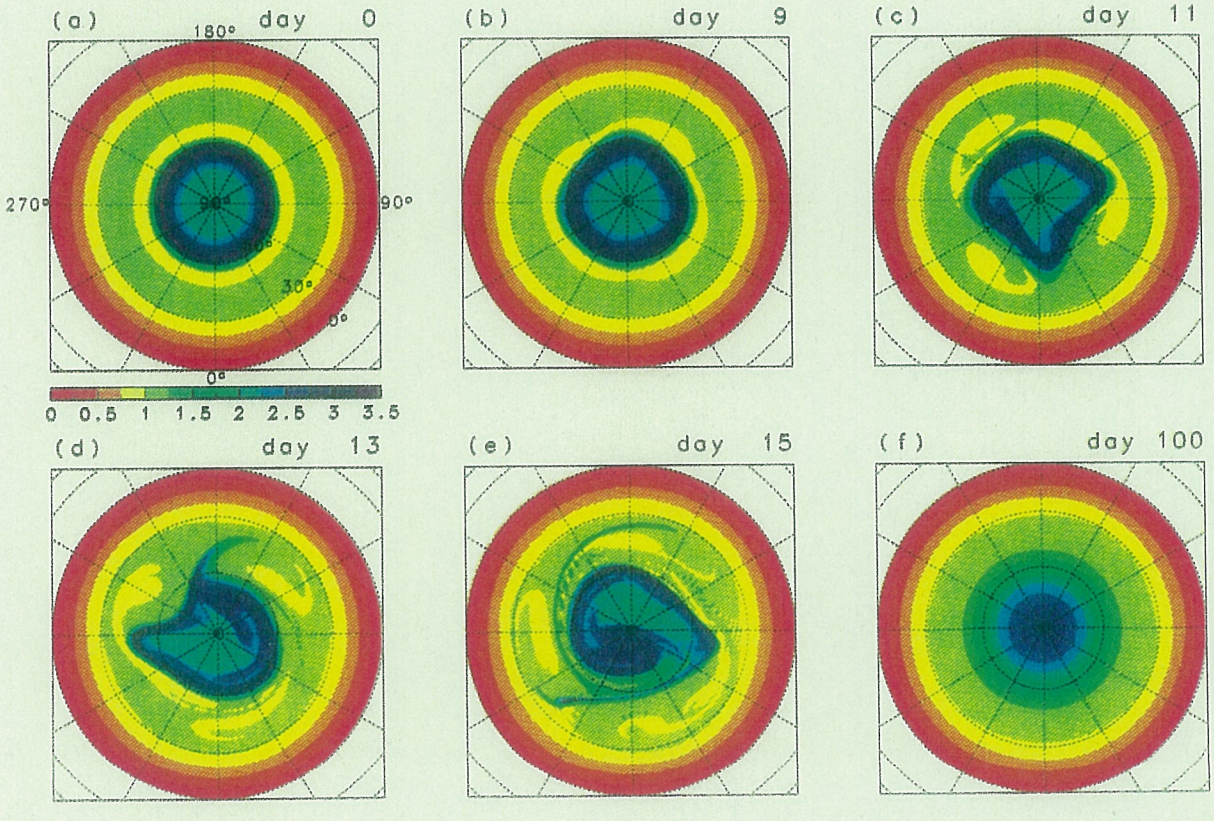

Fig. A2. Same as Fig. A1 except for the sech type jet with $U = 180\,\mathrm{m/s}$, $\varphi_0 = 60°$, and $B = 10°$.

gradient on the poleward side of the jet disappears owing to the equator-ward displacement of the polar fluid with low absolute vorticity (Fig. 9).

2. Decrease of dominant wavenumber is observed in the non-linear phase of the instability for both types of jet. For a wide parameter range of the tanh type jet, Wave 2 exceeds Wave 3 as shown in Fig. 5b–5e and Fig. 6b, 6c although the Wave 3 has the largest growth rate in the linear phase. Similarly, Wave 1 surpasses the most unstable Wave 2 for the case of sech type jet as shown in Fig. 11b.

Acknowledgements

FUJITSU SSL2 Library provided by Data Processing Center, Kyoto University, was used in the eigenvalue analysis, and GFD-DENNOU Library was used for drawing the figures. This work was supported in part by the Grant-in-Aid for Scientific Research, the Ministry of Education, Science, and Culture of Japan, and by the Sumitomo Foundation.

Appendix

Color figures of the absolute vorticity (q) field are used to show two examples of the diagnosis of complicated evolution due to the competition of many unstable modes. The first example is the narrowest jet ($B = 4°$) case of the tanh type jet with $U = 180$ m/s, and $\varphi_0 = 45°$. The corresponding evolution of the zonal and wave energy is shown in Fig. 6a. Figure A1 is the evolution of q field. Initially, there is a belt of very low q (white area) in middle latitudes (a). This region of low q is rolling up into four isolated vortices (b, c). During this roll-up period, the fluid in high latitudes is ejected toward middle latitudes with filament structures. Strong vorticity mixing takes place outside of the vortices in middle latitudes (d, e). Two of the vortices merge around $\lambda \sim 210°$ at Day 10 (e). This evolution reminds us of Fig. 5 in Dritschel and Polvani (1992). In spite of these complicated structures at the beginning of the evolution, the circumpolar vortex becomes nearly zonally symmetric after the accomplishment of vorticity mixing (f).

Figure A2 is the other example of the narrowest sech type jet with $B = 10°$, $U = 180$ m/s and $\varphi_0 = 60°$. The corresponding evolution of the zonal and wave energy is shown in Fig. 11a.

In this case, the initial $\overline{q}$ profile has negative gradients not only in high latitudes but also in middle latitudes (a). Therefore, the vorticity mixing due to the filamentation in middle latitudes occurs as well as the shift of the polar fluid of low q (b–e). Again, the final state is nearly zonally symmetric (f) in spite of these complicated structure at the beginning.

References

Dritschel, D.G. and L.M. Polvani, 1992: The roll-up of vorticity strips on the surface of a sphere. *J. Fluid Mech.*, **234**, 47–69.

Hartmann, D.L., 1976: The structure of the stratosphere in the southern hemisphere during late winter 1973 as observed by satellite. *J. Atmos. Sci.*, **33**, 1141–1154.

Hartmann, D.L., 1983: Barotropic instability of the polar night jet stream. *J. Atmos. Sci.*, **40**, 817–835.

Harwood, R.S., 1975: The temperature structure of the southern hemisphere stratosphere August–October 1971. *Quart. J. R. Meteor. Soc.*, **101**, 75–91.

Holton, J.R., 1989: Global transport processes in the atmosphere. *The handbook of environmental chemistry* Vol. 1 Part E, O. Hutzinger, Ed. Springer Verlag, 97–145.

Juckes, M.N. and M.E. McIntyre, 1987: A high-resolution one-layer model of breaking planetary waves in the stratosphere. *Nature*, **328**, 590–596.

Kuo, H.L., 1949: Dynamic instability of two-dimensional non-divergent flow in a barotropic atmosphere. *J. Met.*, **6**, 105–122.

Kwon, H.J. and M. Mak, 1988: On the equilibration in non-linear barotropic instability. *J. Atmos. Sci.*, **45**, 294–308.

Lait, L.R. and J.L. Stanford, 1988: Fast, long-lived features in the polar stratosphere. *J. Atmos. Sci.*, **45**, 3800–3809.

McIntyre, M.E., 1989: On the antarctic ozone hole. *J. Atmos. Terr. Phys*, **51**, 29–43.

McIntyre, M.E., 1990: Middle atmospheric dynamics and transport: Some current challenges to our understanding. *Dynamics, Transport and Photochemistry in the Middle Atmosphere of the Southern Hemisphere*, Kluwer, 1–18.

Manney, G.L., C.R. Mechoso, L.S. Elson and J.D. Farrara, 1991: Planetary-scale waves in the southern hemisphere winter and early spring stratosphere: stability analysis. *J. Atmos. Sci.*, **48**, 2509–2523.

Manney, G.L., T.R. Nathan and J.L. Stanford, 1988: Barotropic stability of realistic stratospheric jets. *J. Atmos. Sci.*, **45**, 2545–2555.

Manney, G.L., T.R. Nathan and J.L. Stanford, 1989: Barotropic instability of basic states with a realistic jet and a wave. *J. Atmos. Sci.*, **46**, 1250–1273.

Niino, H. and N. Misawa, 1984: An experimental and theoretical study of barotropic instability. *J. Atmos. Sci.*, **41**, 1992–2011.

Polvani, L.M. and R.A. Plumb, 1992: Rossby wave breaking, microbreaking, filamentation, and secondary vortex formation: The dynamics of a perturbed vortex. *J. Atmos. Sci.*, **49**, 462–476.

Prata, A.J., 1984: The 4-day wave. *J. Atmos. Sci.*, **41**, 150–155.

Yoden, S. and K. Ishioka, 1993: A numerical experiment on the breakdown of a polar vortex *J. Meteor. Soc. Japan.*, **71**, 59–72.

順圧不安定な極渦の非線形時間発展

石岡圭一・余田成男
(京都大学理学部地球物理学教室)

成層圏極夜ジェットを理想化した順圧不安定な極渦の非線形時間発展について、幅広い実験パラメター領域で数値実験を行った。その結果、線形安定性解析からは予測されないいくつかの非線形な特徴が見い出された。

まず、絶対渦度場の非線形発展において、2種類の安定化の過程が見られた。すなわち、絶対渦度の逆勾配がジェットより低緯度側にある場合には、細い渦フィラメントの発達に伴う渦度混合によって逆勾配が消滅するのに対し、ジェットより高緯度側にある逆勾配は、極域の絶対渦度が低い気塊が低緯度方向に移動することによって消滅する。

また、中緯度域が不安定となるジェットに対する広いパラメター範囲において、卓越する波の波数の減少が見られた。線形安定性解析における発達率が最大でないにもかかわらず、極渦の安定化の後には東西波数2の東進波が卓越した。